RSC Advances

ROYAL SOCIETY OF CHEMISTRY

www.rsc.org/advances

Journal Name

RSCPublishing

ARTICLE

Charge transfer highways in polymer solar cells embedded with imprinted PEDOT:PSS gratings

Cite this: DOI: 10.1039/x0xx00000x

Chia-Te Yen[a], Fu-Chiao Wu[a], Horng-Long Cheng[a], Hwo-Shuenn Sheu[b], Fu-Ching Tang[c], and Wei-Yang Chou[a,*]

Received 00th January 2012,
Accepted 00th January 2012

DOI: 10.1039/x0xx00000x

www.rsc.org/

This study developed poly(3-hexylthiophene):indene-C_{60} bisadduct (P3HT:ICBA)-based organic solar cells where nanoimprinted poly(3,4-ethylenedioxythiophene): poly(styrenesulfonate) (PEDOT:PSS) gratings successfully functioned as charge transport highways and induced an ICBA-rich surface. The embedded nanostructures improved light harvest and contact area; however, these two factors were not the primary enhancers of solar cell performance. Atomic force microscopy and conductive atomic force microscopy revealed that the imprinted PEDOT:PSS gratings activated hole- and electron-conducting pathways. This result can be attributed to the enhancement of the π–π orbital overlap between P3HT and PEDOT:PSS polymer chains and to the grating-induced ICBA phase separation. These two effects were the primary factors that increased the short-circuit current of the imprinted devices, which resulted in the increase of in power conversion efficiency. In-plane and out-of-plane grazing incident X-ray diffraction revealed that the chain orientation of P3HT on the PEDOT:PSS gratings was the same as that on the plane PEDOT:PSS surface. This study proved the feasibility of nanoimprinting for organic solar cells, even for organic field-effect transistors.

1. Introduction

Organic photovoltaic (OPV) devices have a great potential in energy resource because of their low-cost fabrication, simple process, flexible substrate application, and effective absorption in the solar spectrum. Thus, an increasing number of researchers in the physical and chemical fields concentrated on OPV devices, particularly conjugated polymer-based cells, which can potentially meet the energy demands of the future. Polymer materials can be applied in solution-processed methods and have fast printing processes, which not only enable easy device fabrication but also increase the donor/acceptor (D/A) contact area. The D/A interface is increased by blending. Thus, increasing the D/A contact area is an effective means to enhance the power conversion efficiency (PCE) of solar cells.

Many studies have attempted to improve device efficiency for genuine market impact. This effort, which focused on the materials development and the optimization of each layer for the fabrication processes, has significantly improved OPV efficiency in recent years[1-5]. Embedding of nanostructures in OPV devices is a common method of device modification; this method increases cell efficiency by increasing the contact area, modifying deposited morphology, and improving exciton separation[6-8]. Nanoparticles or nanowires cover the bottom electrode to generate a nanostructure at the interface that can enhance OPV device performance[9-12]. Other methods used in nanostructure fabrication include electron beam writing, scanning probe, ultraviolet-curable nanoimprint lithography[13,14], and thermoplastic nanoimprint lithography (T-NIL)[15-17]. Among these nanotechnologies, T-NIL has the highest viability for commercial-scale OPV fabrication because of its cost effectiveness. However, the conventional T-NIL technique must be conducted under certain pressure and temperature conditions on the target layer to obtain the desired pattern. Characteristic deterioration occurs in some organic materials that cannot sustain the T-NIL fabrication conditions. Thermal expansion mismatch between the mold and the target layer may cause pattern distortion, and sticking of organic materials renders T-NIL molds disposable[18-20].

In this study, we developed a low-temperature and low-pressure NIL process to construct a poly(3,4-ethylenedioxythiophene): poly(styrenesulfonate) (PEDOT:PSS) nanostructure using a soft polydimethylsiloxane (PDMS) mold in poly(3-hexylthiophene):indene-C_{60} bisadduct (P3HT:ICBA) solar cells.[21,22] PEDOT:PSS nanogratings serve as the hole transport layer (HTL). The traditional T-NIL cannot transfer nanogrooves on the PEDOT:PSS surface because PEDOT:PSS lacks a specific glass transition temperature[23]. Results show that the PEDOT:PSS gratings significantly enhance device performance when compared with the standard OPV device whose HTL is a native PEDOT:PSS film. The nanostructure increases light harvest efficiency and contact area. Nevertheless, the absorbance in our imprint sample is lower than the standard case, and the contact area increases by only <1%. Moreover, 2D grazing incidence X-ray scattering (2D GIXS) measurements show that the polymer chain alignment of P3HT is not changed by the nanogratings. For further analyses, we utilized conductive atomic force microscopy (C-AFM) to qualitatively map the charge transport and atomic force microscopy (AFM) to map the surface morphologies of imprinted PEDOT:PSS and P3HT:ICBA. The

imprint devices that exhibit improved short-circuit current relative to standard devices contain a hole-conductive highway at the sidewall of the PEDOT:PSS gratings and an electron-conductive pathway near the surface of the active layer.

2. Experimental methods

2.1. Mold fabrication

PDMS, which serves as an elastic solid after polymerization and cross-linking, was used to form flexible imprinting molds by flowing to cover the surfaces of a Si stamp with nanograting molds[24,25]. This polymeric organosilicon compound is usually used to form imprint molds in soft lithography, which is an advanced technique in transferring nanopatterns onto substrates or polymer surfaces. A self-assembled monolayer (1H, 1H, 2H, 2H - perfluorodecyltrichlorosilane) was thermally deposited onto the surface of the Si stamp as an antiadhesion layer. Two PDMS grating molds, in which one has a width of 600 nm and a pitch of 1200 nm and the other has a width of 1200 nm and a pitch of 2400 nm, were used for nanoimprinting. The soft feature of PDMS molds is expected to enhance imprint yield through particle effect minimization.

2.2. Groove constructed

A 60 nm-thick PEDOT:PSS film was spin-coated onto indium tin oxide (ITO)-coated glass substrates which were sequentially cleaned by sonication bath in detergent, reverse osmosis water, acetone, and 2-propanol, followed by 3 min of 50 W O_2 plasma etching, to increase the surface energy of ITO. Upon the formation of the PEDOT:PSS film on the ITO substrate, nanoimprinting was conducted on the PEDOT:PSS surface at room temperature to construct the nanograting structure (Figure 1). The PEDOT:PSS gratings were heated at 150 °C for 30 min after the substrate was removed from the PDMS mold. A plane PEDOTP:PSS film was also fabricated simultaneously for comparison.

2.3. Device fabrication

OPV cells with a nanostructure configuration of glass/ITO/PEDOT:PSS/P3HT:ICBA/Ca/Al (Figure 1) were fabricated. The blend of P3HT and ICBA acted as the electron donor and the electron acceptor, respectively. A P3HT:ICBA solution was prepared with 1,2-dichlorobenzene (20 mg/mL). The polymer solution was spun at 1400 rpm for 25 s in an N_2-filled glove box, resulting in the formation of a thin film on the PEDOT:PSS gratings. Solvent vapor annealing of the P3HT:ICBA film was conducted in a small moisture-controlled chamber in the glove box. After solvent vapor annealing, the P3HT:ICBA film was baked at 150 °C for 5 min to form the polymer blend film. Cathodes of 20 nm Ca and 100 nm Al were deposited at 5×10^{-6} Torr, defining active areas of 6×10^{-2} cm^2.

2.4. Measurement and analysis

To analyze the influence of the nanoimprinted PEDOT:PSS gratings on OPVs, the current density–voltage (J–V) characteristics of the OPVs were measured in a dark and N_2-filled glove box using an AM 1.5G-filtered Oriel solar simulator at 100 mW/cm^2 calibrated to a standard Si photodiode detector (XP102C). Photocurrent was recorded using a Keithley 2400 source meter. Monochromatic incident photon-to-electron conversion efficiency (IPCE) was measured using a xenon light source through the monochromator to irradiate the OPV devices.

The surface morphologies of the PEDOT:PSS and polymer blend films were analyzed by AFM using a non-contact scanning mold. Figure 1 shows the AFM images of the imprinted and native PEDOT:PSS surfaces, as well as covered polymer surfaces. Meanwhile, C-AFM measurements were conducted using a contact scanning mold to map the carrier injection from the tip on the surface of the active layer. A bias (i.e., ITO electrode) was applied to the bottom layer of the sample, and the Pt-coated tip was maintained at ground potential. The topographic images and current distribution images of the sample were simultaneously recorded through a signal access module. To analyze the hole or electron transport pathway on the surface of the active layer, a positive or negative bias was applied to the sample to control the extraction of electrons or holes from the sample to the tip, respectively.

Considering that the processing conditions of the polymer film would affect the relative intensity of the absorption wavelength for bulk solar cells, we obtained the absorption spectra of the active layer using a Cintra 202 spectrometer. The influence of nanogrooves on the polymer structure was verified by coating the P3HT:ICBA polymer films onto different HTLs, namely, 1200 nm pitch PEDOT:PSS gratings, 2400 nm pitch PEDOT:PSS gratings, and a flat PEDOT:PSS film. All PEDOT:PSS films were used as the

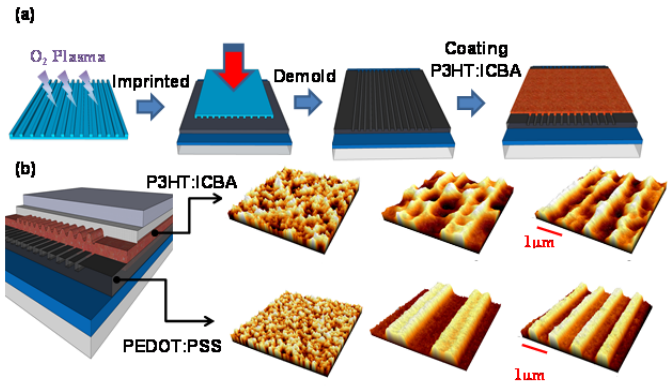

Figure 1. (a) Schematic of the nanoimprinting process. (b) 3D scheme of an OPV with various types of PEDOT:PSS layers. AFM images show the P3HT:ICBA films coated onto native, 1200 nm-wide nanograting-imprinted, and 600 nm-wide nanograting-imprinted PEDOT:PSS surfaces.

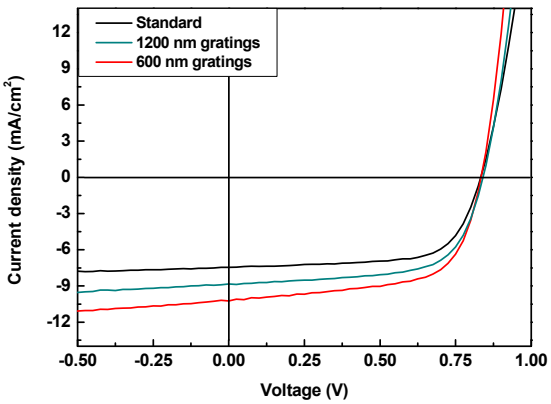

Figure 2. J–V characteristics of P3HT:ICBA OPVs containing native, 600 nm-wide nanograting-imprinted, and 1200 nm-wide nanograting-imprinted PEDOT:PSS layers.

Table 1. Comparison of the photovoltaic parameters of polymer bulk heterojunction solar cells with native PEDOT:PSS layer, as well as 600 nm- and 1200 nm-wide imprinted PEDOT:PSS gratings.

PEDOT:PSS structure	J_{sc} (mA/cm^2)	V_{oc} (V)	*FF*	η (%)	R_{sh} (kΩ · cm^2)
Native	7.40	0.83	0.67	4.11	57.8
1200 nm gratings	8.85	0.84	0.66	4.89	32.2
600 nm gratings	10.24	0.83	0.63	5.40	22.5

background in the absorption measurements. Moreover, 2D GIXS was used to investigate the intermolecular structure of the P3HT:ICBA blend films coated onto imprinted and non-imprinted HTLs. To exclude the broad diffraction signal from the ITO/glass substrate, 2D GIXS was conducted on the blend film that formed on the Si substrate. The 2D GIXS measurements were conducted at the BL-01C02 beamline station of the National Synchrotron Radiation Research Center, Taiwan. The 12 keV beam, that is, a wavelength of 1.0332 Å, had an incident angle of 0.2°, which is close to the critical angle of the substrate. A Mar345 imaging plate area detector was used to collect 2D scattering images. q_{xy} and q_z represent the in-plane and out-of-plane scattering vectors of the blend film, respectively.

3. Results and discussion

The bottom row of Figure 1b shows the topographic images of native and imprinted PEDOT:PSS films that were duplicated from the PDMS mold (AFM scan size: 5 × 5 μm^2). The PEDOT:PSS nanogratings consisted of approximately 60 nm deep, 600 nm- and 1200 nm-wide trenches with pitches of 1200 and 2400 nm, respectively. Oxygen plasma treatment was conducted on the PDMS mold to achieve a hydrophobic surface that simplified demolding. With this treatment, nanoimprinting resulted in pattern transfer fidelity (Figure 1b). The upper row of Figure 1b shows the AFM morphology of the active layers blended with P3HT and ICBA, which were spin-coated onto native and imprinting PEDOT:PSS surfaces. The standard P3HT:ICBA film showed a subtle surface with a roughness of 4.8 nm after a 150 nm-thick P3HT:ICBA film formed onto the native PEDOT:PSS surface. In contrast to the standard P3HT:ICBA film, the P3HT:ICBA film that was spin-coated onto the imprinted PEDOT:PSS gratings preserved the grating morphology on its surface. The roughness of the P3HT:ICBA surface was nearly three times higher than that of the standard P3HT:ICBA film. The contact areas of P3HT:ICBA coated onto 1200 nm- and 600 nm-wide PEDOT:PSS gratings increased by only 0.05% and 0.3%, respectively, when compared with that of P3HT:ICBA coated onto a flat PEDO:PSS surface. Therefore, the contact area between the active layer and the anode may not be the dominant factor influencing current.

Figure 2 shows the photovoltaic outputs of three solar cells with native and imprinted PEDOT:PSS layers. The *J*–*V* curves of the OPV cells were measured on the active area of 0.06 cm^2 under 100 mW/cm^2 light simulation. The performance parameters, namely, PCE, short-circuit current (J_{sc}), open-circuit voltage (V_{oc}), and fill factor (*FF*), of the OPV cells are shown in Table 1. The V_{oc} of the standard and imprinted devices were almost the same. This result can be attributed to the fact that V_{oc} does not depend on the embedded nanostructures but on the difference between the highest occupied molecular orbital of the donor and the lowest unoccupied molecular orbital of the acceptor[26]. The J_{sc} of the devices with 600 nm- and 1200 nm-wide PEDOT:PSS gratings significantly increased

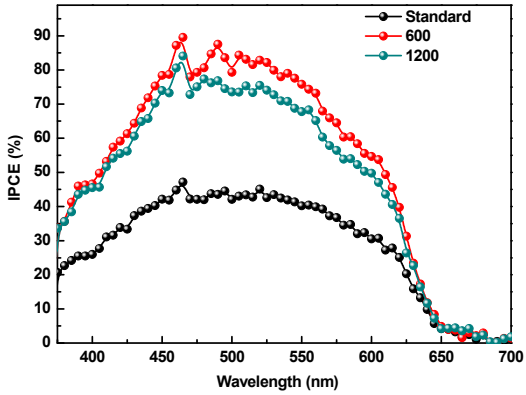

Figure 3. Photoaction spectra of the devices with native and nanostructure PEDOT:PSS layers.

by 38.4% and 19.6%, respectively. Compared with the cell with native PEDOT:PSS layer, lower shunt resistances (R_{sh}) are observed in imprinted cells, indicating that the current losses arise from the nanoimprint PEDOT:PSS gratings. The decrease of R_{sh} results in the slight reduction of FF in imprinted cells. However, the increase in contact area ratio was not proportional to that in J_{sc}. Thus, further studies should be conducted. The PCE of the OPV with 600 nm-wide PEDOT:PSS gratings significantly increased by 31.4%. To verify the key factor that influences OPV device performance, IPCE measurements were first conducted on the three OPV devices. The IPCE spectra of the P3HT:ICBA solar cells with native and imprinted PEDOT:PSS layers are compared in Figure 3. The increase in IPCE for the nanoimprinted devices was almost twice that for the device with the native PEDOT:PSS layer in the visible band. This result indicates that charge carriers can be effectively collected by the imprinted solar cells. However, the device photocurrent was not only affected by the IPCE but also by light absorption intensity.

Figure 4a shows the absorption spectra of the blend films on the native and imprinted PEDOT:PSS layers. The absorbance within the visible range of the blend films on the 600 nm- and 1200 nm-wide PEDOT:PSS nanogratings evidently decreased. However, the J_{sc} of the OPVs with the imprinted PEDOT:PSS layer increased. The absorption tail of P3HT on the nanogratings above 625 nm slightly increased. Accordingly, the large J_{sc} in the imprinted OPVs can be attributed to effective carrier transportation and collection. Several studies expounded that the relative peak intensity of absorption can be used to analyze the structure ordering and conjugation length of polymer chains[27,28]. When the normalization was conducted on Figure 4a, Figure 4b shows that no red shift occurs in the overall absorbance of the P3HT:ICBA films on the imprinted PEDOT:PSS gratings. This result indicates that the nanoimprinting of 600 nm- and 1200 nm-wide PEDOT:PSS gratings did not induce P3HT molecular rearrangements. To further investigate the microstructure of the P3HT films, P3HT crystallization and chain orientation were examined using 2D GIXS measurements (Figure 5a). The scattering intensity recorded using a 2D detector was plotted as a function of the momentum transfer q_z and q_{xy}, which denote directions perpendicular and parallel to the substrate, respectively[29,30]. In-plane and out-of-plane GIXS measurements were obtained simultaneously. Only distinct intensity rods with Bragg reflections along the (100) direction were observed in the 2D GIXS patterns obtained from the P3HT:ICBA films on the native (Figure 5c) and 600 nm-wide grating-imprinted (Figure 5d) PEDOT:PSS surfaces. The (*h*00)

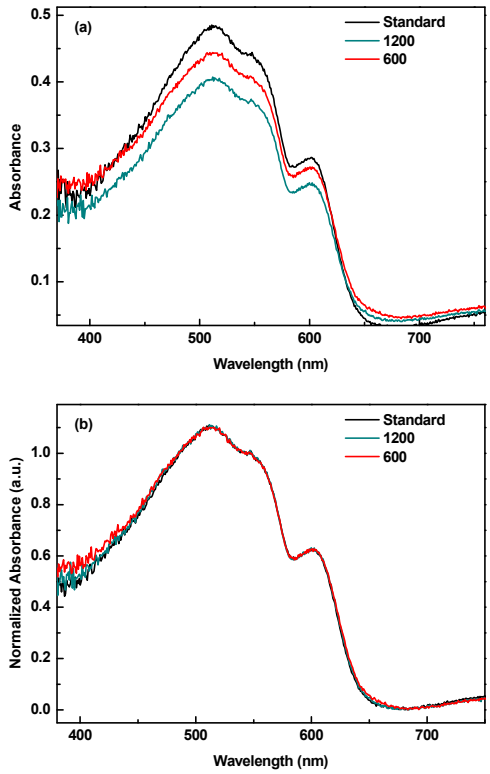

Figure 4. Absorption of P3HT:ICBA blends on native and imprinted PEDOT:PSS/glass substrate. The two types of PEDOT:PSS gratings had 1200 nm pitch, 600 nm width and 2,400 nm pitch, 1200 nm width. For comparison, absorption spectra are shown as (a) absolute intensity and (b) normalized intensity.

peaks corresponded only to the edge-on chain orientation (Figure 5b) existing in all samples, that is, the (100)-axis of lamella structure normal to the substrate[31-33]. The intensity and width at half maximum of (*h*00) up to the third order were almost the same in

both patterns, indicating that the microstructure and arrangement of P3HT cannot be affected by the PEDOT:PSS nanogratings. The AFM images revealed that the PEDOT:PSS gratings changed the morphological features of the active layer. However, the results of GIXS confirmed that the grating structures did not affect the molecular arrangement of P3HT. Figures 5e and 5f show a conceptual model based on the information obtained from absorption and GIXS analyses. The P3HT lamella structure showed the same orientation on the native and imprinted PEDOT:PSS surfaces.

The morphology and the current passing through the tip–P3HT:ICBA junction were simultaneously mapped through C-AFM to investigate the mechanism by which nanoimprinting increases the current of OPV devices[34,35]. This procedure provided a quantitative and direct map of hole transport at the interface between P3HT and PEDOT:PSS. To examine hole transport, only the P3HT solution was spun on the native and imprinted PEDOT:PSS surfaces[36]. We compared the hole transport at the P3HT/PEDOT:PSS grating interface and the P3HT/plane PEDOT:PSS interface because of the same tip–P3HT junction. C-AFM can be used to quantitatively map the hole and electron injection from the tip on the film surface by controlling the negative and positive biases applied to the sample, respectively. When a bias of −1.5 V was applied to the ITO contact, holes were injected from the sharp tip. Accordingly, the C-AFM

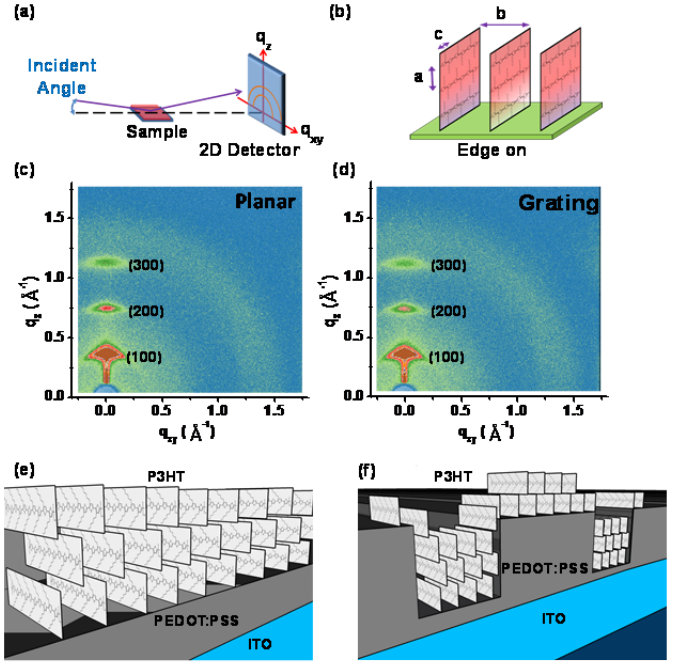

Figure 5. (a) Schematic of the GIXS setup for in-plane and out-of-plane measurements. (b) Schematic of the orientation of P3HT chains on the PEDOT:PSS surface. Reciprocal map of P3HT:ICBA films on (c) native PEDOT:PSS surface and (d) imprinted PEDOT:PSS nanogratings with 600 nm width and 1200 nm pitch measured by GIXS using a 2D detector. Schematic of the orientation of P3HT chains on (e) native PEDOT:PSS and (f) imprinted PEDOT:PSS grating surfaces.

images show the most current, where hole injection and transport were predominant. Figures 6a and 6b show the surface morphology and current image of a pristine P3HT film coated onto imprinted 600 nm-wide PEDOT:PSS gratings, respectively. The morphology of the gratings was preserved on the P3HT film surface. Comparison of the morphology and current images revealed prevalent current located near the PEDOT:PSS gratings. To identify the precise location of the prevalent current, cross-sectional views of the morphology and current images were obtained. Figure 6c shows the 1D topography and current image along the direction perpendicular to the gratings. Notably, the current was significantly enhanced on the sidewall of the gratings, indicating that the sidewalls of the nanogratings were preferentially hole-conducting pathways. By contrast, hole transport on top of the PEDOT:PSS gratings was difficult. To examine the effect of nanoimprinting on hole transport, negative-biased C-AFM measurements were also conducted on the standard P3HT film, which was formed on the native PEDOS:PSS surface. Figures 6d and 6e show the surface topography and the current image of the standard P3HT film, respectively. Current distribution on the standard P3HT film revealed a less direct correlation with the surface morphology. Comparison of the imprinted and standard cases showed that the maximum magnitude of the current transport was 95 pA in the imprinted sample and only 45 pA (average value obtained based on Figure 6f) in the standard sample, which was almost the same as the current transported on top of the PEDOT:PSS gratings (Figure 6c). The average value of hole current transported from P3HT to the imprinted PEDOT:PSS was 66 pA. This 1.5-fold increase in current as determined by C-AFM corresponded with the increase in J_{sc} in the imprinted OPV. Thus, we can attribute the hole current increase to an overlap of conjugated π orbitals between P3HT and PEDOT:PSS, as shown in the conceptual model depicted

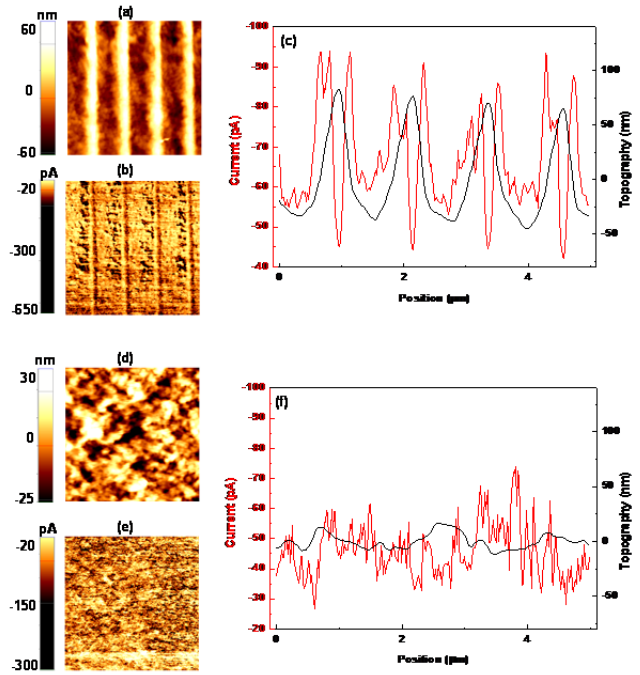

Figure 6. AFM topography of the P3HT film formed on PEDOT:PSS gratings with 1200 nm pitch, 600 nm width, and 60 nm depth (a) and corresponding C-AFM map at a bias of −1.5 V (b) and corresponding 1D morphology and current distribution (c). A standard P3HT topography (d) and corresponding C-AFM map at a bias of −1.5 V (e) and corresponding 1D morphology and current distribution (f).

in Figure 5f. This π–π overlap facilitated an efficient hole transport for P3HT on the PEDOT:PSS gratings, indicating that the sidewall regions were preferentially hole-conducting pathways, *i.e.* enhancement of the hole mobility of P3HT/ICBA blend film, as shown in Figure S1 and Table S1. By contrast, small currents passed through the grating tops and trench bottoms because of the lesser π–π overlap in these regions than in the sidewall.

Figures 7a, 7b, and 7c show the topographies of P3HT:ICBA films coated onto native, 1200 nm-wide grating-imprinted, and 600 nm-wide grating-imprinted PEDOT:PSS surfaces, respectively, with corresponding current maps in Figures 7d, 7e, and 7f at a bias of +1.5 V. An indistinct grating morphology was observed on the P3HT:ICBA films formed on the PEDOT:PSS gratings. Under positive bias, electrons were injected through the tip. The electron prevalent C-AFM images showed a high current[37,38], indicating ICBA abundance. Comparison of the three current maps (Figures 7d, 7e, and 7f) showed that the highest current occurred at the sample with 600 nm-wide PEDOT:PSS gratings. This result indicates that the vertical phase separation and the formation of ICBA-rich surface layer were induced by the nanoimprinted PEDOT:PSS gratings. A similar phenomenon was observed in the sample with 1200 nm-wide PEDOT:PSS gratings. The number of pixels as a function of current magnitude was statistically compiled to measure the current distribution on the C-AFM maps (Figure 7g). The sample with 600 nm-wide imprinted PEDOT:PSS gratings had the highest current and the largest current distribution among the three maps, indicating that the electrons were easily injected from the tip into the P3HT:ICBA film. This result was attributed to the ICBA-rich surface and uniform ICBA distribution. Accordingly, the imprinted PEDOT:PSS gratings

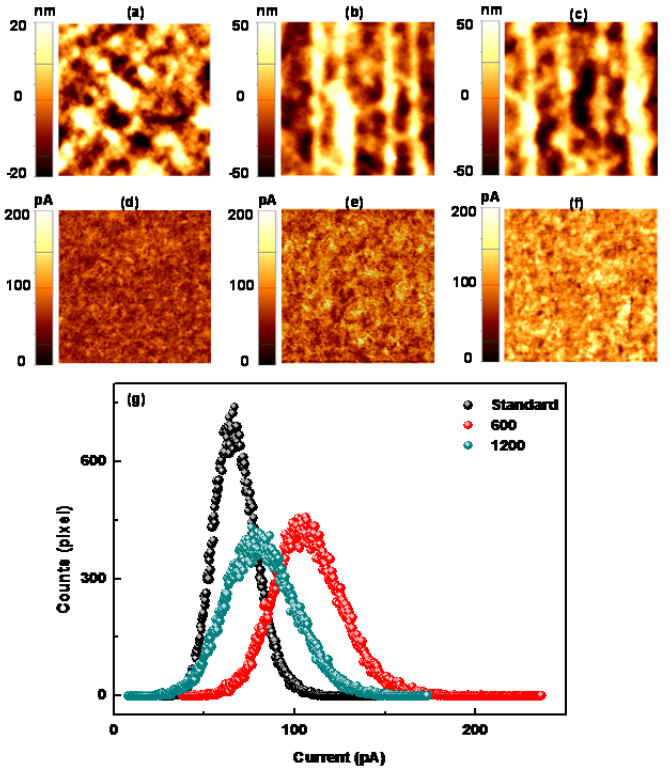

Figure 7. AFM images of P3HT:ICBA blend films formed on (a) native PEDOT:PSS surface, (b) PEDOT:PSS gratings with 2400 nm pitch, 1200 nm width, and 60 nm depth, and (c) PEDOT:PSS gratings with 1200 nm pitch, 600 nm width, and 60 nm depth, as well as corresponding C-AFM maps of the blends coated onto (d) native, (e) 1200 nm-wide grating-imprinted, and (f) 600 nm-wide grating-imprinted PEDOT:PSS. (g) Statistics of current distribution for the three C-AFM maps.

induced phase separation that contributed to carrier transport and collection on both cathodes. The large ICBA distribution within the surface region of the active layer enhanced the electron transport because of the acceptor near the cathode. These C-AFM results can be used to explain the enhanced IPCE of the OPVs after blending nanoimprints on the HTL, that is, the PEDOTP:SS layer. Thus, nanoimprinting may be further used in another layer of OPVs, such as the active layer and the electron transport layer, which can improve hole and electron transports and extractions, even light harvest.

4. Conclusions

The phase separation and carrier collection of P3HT:ICBA blends by nanoimprint lithography for organic solar cells were investigated using C-AFM. To improve the efficiency of organic solar cells, nanoimprinted PEDOT:PSS gratings with widths of 600 and 1200 nm were formed as the HTL. As the P3HT:ICBA film was coated onto the imprinted PEDOT:PSS gratings, a preferentially hole-conducting pathway was established on the sidewall of the gratings because of the enhancement of the π–π orbital overlap between the P3HT and PEDOT:PSS polymer chains. Moreover, phase separation was induced by PEDOT:PSS gratings to yield a ICBA-rich surface that enhances electron transport from the blend film to the cathode. The J_{sc} of the devices with PEDOT:PSS grating widths of 600 and 1200 nm increased by 38.4% and 19.6%, respectively. The grating

morphology was correlated with electrical characteristics by quantitative C-AFM and GIXS measurements. Although the light absorption of the imprinted device was smaller than that of the standard device, large IPCE and photocurrent were observed for the imprinted device. The large IPCE and photocurrent were associated with the improvement of local hole transport pathways on the grating sidewalls and with the enhancement of electron transport induced by the ICBA-rich surface. These hole-conducting pathways and ICBA phase separation were directly proven by C-AFM measurements. The GIXS and normalized absorption spectra indicated that the imprinted PEDOT:PSS nanogratings increased the π–π interchain interactions and phase separation but did not change the microstructure of chain alignment within P3HT:ICBA blend films. Thus, the nanograting-embedded structure can enhance charge transport, including holes and electrons, in organic solar cells. Moreover, the nanoimprinting experiment was simple and extremely fast. These nanostructures can also be used to enhance the charge carrier mobility of field-effect transistors[39].

Acknowledgements

The authors acknowledge financial support from the Ministry of Science and Technology, Taiwan, through Grant NSC 102-2112-M-006-002-MY3. The assistance of the Center for Micro/Nano Technology Research, National Cheng Kung University, for support through equipment and cooperation is gratefully acknowledged.

Notes and references

[a] *Department of Photonics, Advanced Optoelectronic Technology Center, National Cheng Kung University, Tainan 701, Taiwan. E-mail: weiyang@mail.ncku.edu.tw; Fax: +886 6 2095040; Tel: +886 6 2757575 ext.63912*
[b] *National Synchrotron Radiation Research Center, Hsinchu 300, Taiwan .*
[c] *Department of Physics, National Cheng Kung University, Tainan 701, Taiwan.*

1. Z. C. He, C. M. Zhong, S. J. Su, M. Xu, H. B. Wu and Y. Cao, *Nat Photonics*, 2012, **6**, 591.
2. S. J. Liu, K. Zhang, J. M. Lu, J. Zhang, H. L. Yip, F. Huang and Y. Cao, *J Am Chem Soc*, 2013, **135**, 15326.
3. T. B. Yang, M. Wang, C. H. Duan, X. W. Hu, L. Huang, J. B. Peng, F. Huang and X. Gong, *Energ Environ Sci*, 2012, **5**, 8208.
4. J. B. You, L. T. Dou, K. Yoshimura, T. Kato, K. Ohya, T. Moriarty, K. Emery, C. C. Chen, J. Gao, G. Li and Y. Yang, *Nat Commun*, 2013, **4**.
5. C. E. Small, S. Chen, J. Subbiah, C. M. Amb, S. W. Tsang, T. H. Lai, J. R. Reynolds and F. So, *Nat Photonics*, 2012, **6**, 115.
6. Y. Yang, K. Mielczarek, M. Aryal, A. Zakhidov and W. Hu, *Acs Nano*, 2012, **6**, 2877.
7. W. Y. Chou, J. Chang, C. T. Yen, F. C. Tang, H. L. Cheng, M. H. Chang, S. L. C. Hsu, J. S. Chen and Y. C. Lee, *Appl Phys Lett*, 2011, **99,** 183108.
8. W. H. Baek, I. Seo, T. S. Yoon, H. H. Lee, C. M. Yun and Y. S. Kim, *Sol Energ Mat Sol C*, 2009, **93**, 1587.
9. C. Y. Kuo and C. Gau, *Appl Phys Lett*, 2009, **95**, 053302.
10. P. M. Sirimanne, E. V. A. Premalal and H. Minoura, *Renew Energ*, 2011, **36**, 405.
11. D. Y. Liu, M. Y. Zhao, Y. Li, Z. Q. Bian, L. H. Zhang, Y. Y. Shang, X. Y. Xia, S. Zhang, D. Q. Yun, Z. W. Liu, A. Y. Cao and C. H. Huang, *Acs Nano*, 2012, **6**, 11027.
12. W. Kylberg, F. A. de Castro, P. Chabrecek, T. Geiger, J. Heier, P. G. Nicholson, F. Nuesch, E. Theocharous, U. Sonderegger and R. Hany, *Prog Photovoltaics*, 2013, **21**, 652.
13. K. Soderstrom, J. Escarre, O. Cubero, F. J. Haug, S. Perregaux and C. Ballif, *Prog Photovoltaics*, 2011, **19**, 202.
14. M. A. G. Lazo, R. Teuscher, Y. Leterrier, J. A. E. Manson, C. Calderone, A. Hessler-Wyser, P. Couty, Y. Ziegler and D. Fischer, *Sol Energ Mat Sol C*, 2012, **103**, 147.
15. G. Leising, B. Stadlober, U. Haas, A. Haase, C. Palfinger, H. Gold and G. Jakopic, *Microelectron Eng*, 2006, **83**, 831.
16. Y. C. Lee, S. C. Yeh, Y. Y. Chou, P. J. Tsai, J. W. Pan, H. M. Chou, C. H. Hou, Y. Y. Chang, M. S. Chu, C. H. Wu and C. H. Ho, *Microelectron Eng*, 2013, **105**, 86.
17. N. Sanetra, Z. Karipidou, R. Wirtz, N. Knorr, S. Rosselli, G. Nelles, A. Offenhaeusser and D. Mayer, *Adv Funct Mater*, 2012, **22**, 1129.
18. M. R. Cavallari, V. R. Zanchin, M. Pojar, A. C. Seabra, M. D. Pereira-da-Silva, F. J. Fonseca and A. M. De Andrade, *J Electron Mater*, 2014, **43**, 1317.
19. H. Y. Tseng, W. F. Chen, C. K. Chu, W. Y. Chang, Y. Kuo, Y. W. Kiang and C. C. Yang, *Nanotechnology*, 2013, **24**, 065102.
20. C. M. Bates, M. A. B. Pantoja, J. R. Strahan, L. M. Dean, B. K. Mueller, C. J. Ellison, P. F. Nealey and C. G. Willson, *J Polym Sci Pol Chem*, 2013, **51**, 290.
21. G. J. Zhao, Y. J. He and Y. F. Li, *Adv Mater*, 2010, **22**, 4355
22. J. B. You, L. T. Dou, K. Yoshimura, T. Kato, K. Ohya, T. Moriarty, K. Emery, C. C. Chen, J. Gao, G. Li and Y. Yang, *Nat Commun*, 2013, **4**, 1446
23. T. A. Skotheim, J. Reynolds, in Conjugated Polymers: Processing and Applications, CRC Press,USA, 3rd edn., 2006, ch 2, pp. 3.
24. J. Y. Li, Y. C. Ho, Y. C. Chung, F. C. Lin, W. L. Liao and W. B. Tsai, *Biofabrication*, 2013, **5**, 035003.
25. F. Hua, Y. G. Sun, A. Gaur, M. A. Meitl, L. Bilhaut, L. Rotkina, J. F. Wang, P. Geil, M. Shim, J. A. Rogers and A. Shim, *Nano Lett*, 2004, **4**, 2467.
26. C. J. Brabec, A. Cravino, D. Meissner, N. S. Sariciftci, T. Fromherz, M. T. Rispens, L. Sanchez and J. C. Hummelen, *Adv Funct Mater*, 2001, **11**, 374.
27. J. F. Chang, J. Clark, N. Zhao, H. Sirringhaus, D. W. Breiby, J. W. Andreasen, M. M. Nielsen, M. Giles, M. Heeney and I. McCulloch, *Phys Rev B*, 2006, **74**, 115318.
28. H. L. Cheng, J. W. Lin, F. C. Wu, W. R. She, W. Y. Chou, W. J. Shih and H. S. Sheu, *Soft Matter*, 2011, **7**, 351.
29. Y. Kim, S. Cook, S. M. Tuladhar, S. A. Choulis, J. Nelson, J. R. Durrant, D. D. C. Bradley, M. Giles, I. Mcculloch, C. S. Ha and M. Ree, *Nat Mater*, 2006, **5**, 197.
30. R. J. Kline and M. D. McGehee, *Polym Rev*, 2006, **46**, 27.
31. M. Aryal, K. Trivedi and W. C. Hu, *Acs Nano*, 2009, **3**, 3085.
32. X. T. Hao, T. Hosokai, N. Mitsuo, S. Kera, K. K. Okudaira, K. Mase and N. Ueno, *J Phys Chem B*, 2007, **111**, 10365.
33. H. Sirringhaus, P. J. Brown, R. H. Friend, M. M. Nielsen, K. Bechgaard, B. M. W. Langeveld-Voss, A. J. H. Spiering, R. A. J. Janssen, E. W. Meijer, P. Herwig and D. M. de Leeuw, *Nature*, 1999, **401**, 685.
34. Y. P. Jiang, Q. Qi, R. Wang, J. Zhang, Q. K. Xue, C. Wang, C. Jiang and X. H. Qiu, *Acs Nano*, 2011, **5**, 6195.
35. C. Ionescu-Zanetti, A. Mechler, S. A. Carter and R. Lal, *Adv Mater*, 2004, **16**, 385.
36. P. Dutta, Y. Xie, M. Kumar, M. Rathi, P. Ahrenkiel, D. Galipeau, Q. Q. Qiao and V. Bommisetty, *J Photon Energy*, 2011, **1**, 011124.
37. D. Martin, M. Grube, P. Reinig, L. Oberbeck, J. Heitmann, W. M. Weber, T. Mikolajick and H. Riechert, *Appl Phys Lett*, 2011, **98**, 012901.
38. T. A. Bull, L. S. C. Pingree, S. A. Jenekhe, D. S. Ginger and C. K. Luscombe, *Acs Nano*, 2009, **3**, 627.
39. W. Y. Chou, M. H. Chang, H. L. Cheng, S. P. Yu, Y. C. Lee, C. Y. Chiu, C. Y. Lee and D. Y. Shu, *Appl Phys Lett*, 2010, **96**.083305.

Table of Contents

Charge transfer highways in polymer solar cells embedded with imprinted PEDOT:PSS gratings

*Chia-Te Yen, Fu-Chiao Wu, Horng-Long Cheng, Hwo-Shuenn Sheu, Fu-Ching Tang, and Wei-Yang Chou**

Carrier transport highways induced by nanoimprinted PEDOT:PSS gratings play important roles in enhancement of electrical performances of P3HT:ICBA-based organic photovoltaic cells.